We are IntechOpen, the world's leading publisher of Open Access books Built by scientists, for scientists

4,800
Open access books available

122,000
International authors and editors

135M
Downloads

Our authors are among the

154
Countries delivered to

TOP 1%
most cited scientists

12.2%
Contributors from top 500 universities

CLARIVATE ANALYTICS BOOK CITATION INDEX INDEXED

WEB OF SCIENCE™

Selection of our books indexed in the Book Citation Index in Web of Science™ Core Collection (BKCI)

Interested in publishing with us?
Contact book.department@intechopen.com

Numbers displayed above are based on latest data collected.
For more information visit www.intechopen.com

4

A novel all-solid-state thin-film-type lithium-ion battery with in-situ prepared electrode active materials

Yasutoshi Iriyama
Shizuoka University
Japan

1. Introduction

All-solid-state thin-film rechargeable lithium batteries have received much attention as a power source for micro devices. Especially, in recent years, thin-film batteries using lithium phosphorus oxynitride glass electrolyte (LiPON) discovered by Wang and co-workers (Wang et al., 1996) have been extensively investigated. In the fabrication process of these film batteries, thin films of electrodes, solid electrolyte, and current collectors are sequentially piled-up on a substrate using different kinds of vapor deposition techniques such as pulsed laser deposition, r.f. magnetron sputtering, and vacuum evaporation.
For the practical application of thin-film batteries, the fabrication process is desirable to be simplified as much as possible. One of the effective methods to overcome the above problem will be the use of ''*in-situ* formed'' material in the battery system. Using this in situ formed material, fabrication of at least one of the material in a battery will not be necessary, leading to both the simplification and cost reduction for its fabrication process. The use of ''in situ formed'' solid electrolyte have been already shown in a primary battery system of Li/poly-2-vinylpyridide (P2VP)•I_2 (Greatbatch et al., 1971), which was commercialized as power sources of cardiac pacemakers. In this battery system, solid electrolyte of LiI was prepared at the negative electrode/positive electrode interface through the reaction of these electrodes. Neudecker et al. have proposed ''Lithium-free'' thin-film rechargeable lithium battery using LiPON, where electrochemically plated Li was used as an in situ formed anode material (Neudecker et al., 2000). Because of high reactivity of Li, the battery system required an overlayer to prevent side reactions with the Li anode. Lee et al. proposed a reversed structural configuration of the lithium-free battery so that the overlayer was not required. Although the use of in situ formed Li anode is very attractive to simplify the fabrication process, this battery system relies on specific stability of LiPON against lithium metal.
Most of oxide-based solid electrolyte dose not obtain such stability against lithium metal and then this technique will not be used to these solid electrolytes. It is well known that there are so many oxide-based solid electrolytes containing transition metal ions. It should be noted that some of these solid electrolytes can act as an electrode material when the electrode potential exceed their voltage windows. For example, $Li_3xLa_{(2/3)-x}TiO_3$($0.04 < x < 0.16$) (LLT) with ABO_3-perovskite structure can be an insertion electrode material after

reductive decomposition (Birke et al., 1997). When such a decomposition reaction is partially conducted in the solid electrolyte, decomposition product can be in situ formed electrode material combined with the solid electrolyte, that can be an unit of all-solid-state battery system. Based on the above concept, this chapter will introduce a possibility to fabricate an all-solid-state thin-film-type lithium-ion battery with in situ formed electrode material. In the next section, inorganic solid electrolytes, especially, oxide-based solid electrolyte including transition metals will be briefly summarized, and two examples of reductive decomposition reaction of solid electrolytes will be picked-up. Finally, examples of all-solid-state thin-film-type batteries with in-situ formed electrode active materials will be introduced.

2. Solid Electrolytes and their decomposition reaction

2.1 Lithium-ion conducting solid electrolytes

Lithium-ion conducting solid electrolytes used for all-solid-state rechargeable lithium batteries should provide the following electrical and physical properties in general.

1. High lithium-ion conductivity with negligible electronic conductivity at operating temperature, preferably at room temperature.
2. Wide potential window at both positive and negative electrode sides: sufficient stability against chemical reaction with both electrodes.
3. Environmentally benign, nonhygroscopic, low cost, and ease of preparation.

	Lithium-ion conductors	σ_{ionic} / S cm^{-1} (at R.T.)	Researchers	Year
①	LiI	1 x 10^{-7}	Ginnings and Phipps	1930
②	Li-βAl_2O_3	3 x 10^{-3}	Yao and Kummer	1967
③	Li_3N	10^{-3}	Alpen and Muller	1977
④	$Li_{14}Zn(GeO_4)_4$ (LISICON)	2 x 10^{-6} (at 323 K)	Hong	1978
⑤	4.9LiI-34.1Li_2O-61B_2O_3	2 x 10^{-7}	Malgani and Robert	1979
⑥	$Li_{3.6}Ge_{0.6}V_{0.4}O_4$	4 x 10^{-5}	Kuwano and West	1980
⑦	0.30Li_2S-0.26B_2S_3 -0.44LiI	1.7 x 10^{-3}	Wada *et al.*	1983
⑧	$LiTi_2(PO_4)_3$	2 x 10^{-6}	Subramanian *et al.*	1986
⑨	60Li_2S-40SiS_2	4 x10^{-4}	Pradel and Ribes	1986
⑩	$Li_{1.3}Al_{0.3}Ti_{1.7}(PO_4)_3$	7 x 10^{-4}	Aono *et al.*	1989
⑪	0.02Li_3PO_4-0.98(Li_2S-SiS_2)	7.6 x 10^{-4}	Takada *et al.*	1993
⑫	$Li_{0.35}La_{0.55}TiO_3$ (LLT)	1 x 10^{-3}	Inaguma *et al.*	1993
⑬	$Li_{2.9}PO_{3.3}N_{0.46}$ (LiPON)	2 x 10^{-6}	Bates *et al.*	1993
⑭	2[$Li_{1.4}Ti_2Si_{0.4}P_{2.6}O_{12}$]-$AlPO_4$	1.5 x 10^{-3}	Fu	1997
⑮	$Li_{3.25}Ge_{0.25}P_{0.25}S_4$ (Thio-LISICON)	2.2 x 10^{-3}	Kanno and Maruyama	2001
⑯	0.7Li_2S ·0.3P_2S_5 glass-ceramics	3.2 x 10^{-3}	Mizuno *et al.*	2005

Table 1. Ionic conductivities of typical inorganic lithium-ion conductors.

Assuming that "solid electrolytes" are defined as lithium-ion conductors that are present in solid state in the macroscopic view, polymer or gel electrolytes will be included in the category. These electrolytes are excellent in terms of flexibility and ease of preparation. However, this chapter focuses on inorganic solid electrolyte mainly including transition metal oxides in them. Table 1 summarizes such inorganic lithium-ion conductors reported to

date. Figure 1 shows the temperature dependence of ionic conductivities for these conductors. Several kinds of conductors, such as Li-βAl_2O_3 (Yao and Kummer, 1967) and Li_3N (Rabenau, A., 1982), show high ionic conductivities (larger than 10^{-3} S cm^{-1}) even at room temperature, comparable to that of the currently used liquid or gel electrolytes in lithium-ion batteries. However, they are not simply used as solid electrolytes for lithium batteries because of their chemical instability. For example, Li_3N has a low decomposition potential (0.445 V (vs Li/Li^+)) so that its application to all-solid-state batteries is limited.

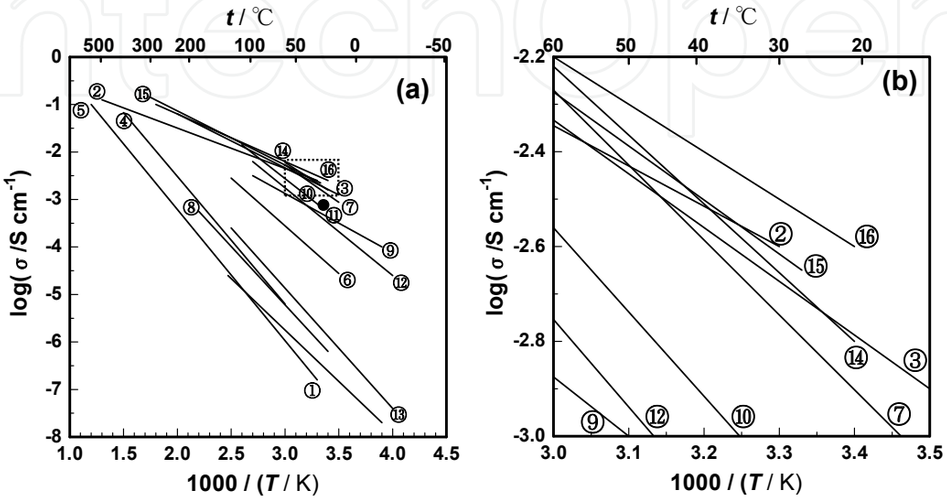

Fig. 1. (a)Temperature dependence of ionic conductivities for typical solid state lithium-ion conductors listed in Table 1. Dotted box in panel (a) is enlarged in panel (b).

Crystalline oxide-based inorganic solid electrolytes with higher chemical stability have been explored since the late 1970s. The material design of crystalline oxide-based ionic conductors is based on certain structural criteria: (i) mobile ions should have suitable sizes for conduction pathways in the lattice and (ii) there should be disorder in the mobile ion sublattice. Based on these considerations, solid solutions of Li_4GeO_4–Li_3VO_4, which is isostructural to $Li_{14}Zn(GeO_4)_4$ (lithium super ionic conductor; LISICON) (Hong 1978) related to the γ-Li_3PO_4 structure, were synthesized (Kuwano and West, 1980). Partial substitution of Li_4GeO_4 by Li_3VO_4 induced vacancies in the lithium sites, resulting in easier lithium-ion hopping in the structure. The substituted $Li_{3.6}Ge_{0.6}V_{0.4}O_4$ crystal attained ionic conductivity of 4×10^{-5} S cm^{-1} at room temperature, which were a few orders higher than those of the members. Another example is lithium lanthanum titanate, $Li_{3x}La_{(2/3)-x}TiO_3$ ($0.04 < x < 0.16$) (LLT) with ABO_3-perovskite structure (Inaguma et al., 1993). LLT showed high ionic conductivity, on the order of 10^{-3} S cm^{-1}, taking advantage of favorable lithium-ion hopping via *A*-sites in the perovskite structure.

Oxyacid-based solid electrolyte, typically $LiM_2(PO_4)_3$ (*M* = Ti (Subramanian et al., 1986), Fe (Sigaryov and Terziev, 1993), ...) compounds with NASICON (sodium (Na) super ionic conductor) structure, have been investigated progressively as solid electrolytes. Partial substitution of tetravalent M^{4+} ions in the $LiM_2(PO_4)_3$ by pentavalent A^{5+} ions or trivalent B^{3+} ions induced lithium-deficient $Li_{1-x}M_{2-x}A_x(PO_4)_3$ compounds or lithium-excess $Li_{1+x}M_{2-x}B_x(PO_4)_3$ compounds, respectively, which effectively enhance their ionic conductivities. Although the NASICON-based materials showed rather high ionic conductivities in the

bulk, they also exhibited large grain boundary resistances. To solve these problems, the M ions were partially substituted by Al or Sc, which enhanced the degree of sintering and increased the ionic conductivity at grain boundaries (Aono et al., 1989, 1990). The resultant $Li_{1.3}Ti_{1.7}Al_{0.3}(PO_4)_3$ showed the highest ionic conductivity among the NASICON-based materials, 7×10^{-4} S cm^{-1}. Taking advantage of the high ionically conductive $Li_{1.3}Ti_{1.7}Al_{0.3}(PO_4)_3$ phase mentioned above, Fu synthesized $Li_2O–Al_2O_3–TiO_2–P_2O_5$ glass ceramics showing ionic conductivity of 1.3×10^{-3} S cm^{-1} without grain boundary resistance (Fu, 1997). He subsequently optimized the elemental composition and reported in 1997 that $2[Li_{1.4}Ti_2Si_{0.4}P_{2.6}O_{12}]$-$AlPO_4$ glass-ceramics exhibited 1.5×10^{-3} S cm^{-1} at room temperature.

Oxide-based glassy materials have also been well studied as lithium-ion conducting solid electrolytes. They exhibit several advantages over crystalline electrolytes; in particular, they can provide isotropic ionic conduction without grain boundary resistance because of their random open framework. Development of oxide-based glassy electrolytes has been conducted based on the following two approaches. One is based on the LiX-Li_2O-M_xO_y (M_xO_y = B_2O_3, P_2O_5, GeO_2) glass system, which is an analog of lithium substitution of super silver-ion conducting glasses, AgX-Ag_2O-M_xO_y, showing over 10^{-2} S cm^{-1} at room temperature. For example, $LiI–Li_2O–B_2O_3$ showed ionic conductivity of 10^{-7} S cm^{-1} (Malugani and Robert, 1979). Another approach stems from the discovery that rapid-quenched glasses of ferroelectric $LiNbO_3$ crystals showed high ionic conductivity of 10^{-5} S cm^{-1} (Glass et al., 1978). Based on this discovery, various kinds of oxyacid glasses have been synthesized. These include $Li_4SiO_4–Li_3BO_3$, $Li_2O–SiO_2–_2O_3$, and $Li_2O–SiO_2–ZrO_2$. Lithium phosphorus oxynitride (LiPON) glasses showed acceptable ionic conductivity (2×10^{-6} S cm^{-1}) when used for thin-film batteries (Bates et al., 1993). The LiPON glasses showed chemical stability against lithium metal because of their structural stability, originating from the introduction of nitrogen ions into the structure. The outstanding features of LiPON glass electrolytes have encouraged many researchers to study all-solid-state thin-film rechargeable lithium batteries using this solid electrolyte.

2.2 Decomposition of solid electrolyte and their lithium insertion/extraction reaction

As mentioned above, there have been many studies on the development of solid electrolytes, and various kinds of solid electrolyte have been discovered. It should be noted that there are many solid electrolytes containing 3*d*-transition metal ions: *e.g.*, V^{5+} in $Li_{3.6}Ge_{0.6}V_{0.4}O_4$ (Kuwano and West, 1980), Ti^{4+} in $Li_{1.3}Ti_{1.7}Al_{0.3}(PO_4)_3$ (Aono et al., 1989), $Li_{3x}La_{2/3-x}TiO_3$ (LLT) (Inaguma et al., 1993) and $2[Li_{1.4}Ti_2Si_{0.4}P_{2.6}O_{12}]$-$AlPO_4$ (Fu, 1997). These solid electrolytes are intrinsically susceptible to reductive decomposition accompanied by redox reactions of the transition metal ions through Li^+ insertion into them. It should be noted that transition metal oxides, such as CoO, FeO, NiO, etc, can work as high voltage negative electrode materials through conversion reaction (Poizot et al., 2000). Also, TiO_2 is well-known lithium insertion electrode material. In other words, when these transition metal oxides are prepared electrochemically in solid electrolyte vir the reductive decomposition reaction of solid electrolytes, the resultant material will work as electrode active materials. Moreover, because the decomposed material is grown from solid electrolytes, electrode/solid electrolyte interface with good adhesion can be simply prepared in principle. It is expected that success of such novel interface design become a breakthrough to develop advanced all-solid state battery system with low-cost and much smaller internal resistance. In this section, two examples of reductive decomposition of solid electrolytes will be introduced.

2.2.1 Li-V-Si-P-O system

An amorphous Li_2O–V_2O_5–SiO_2 system in which Li_2O and SiO_2 are expected to have a function as network modifier and network former, respectively, to stabilize the amorphous material. This system has been initially noted as a solid electrolyte in an analog of Li_3VO_4–Li_4SiO_4 solid solution. Bulk crystals of $Li_{3.4}V_{0.6}Si_{0.4}O_4$ with a γ-Li_3PO_4 structure, which is isostructural to the so-called lithium superionic conductor "LISICON" showed high ionic conductivity of 1 x 10^{-5} S cm^{-1} with negligible electronic conductivity at room temperature, which has encouraged several researchers to study all-solid-state batteries using this solid electrolyte. Thin solid electrolyte films of the Li–V–Si–O system have been reported to show acceptable ionic conductivity as an application for all-solid-state thin-film batteries. Partially crystallized Li–V–Si–O thin films have been prepared by r.f. magnetron sputtering (Ohtsuka and Yamaki, 1989) and amorphous one have been by pulsed laser deposition (PLD) (Kawamura et al., 2004). These film electrolytes have been successfully used in all-solid-state thin-film batteries. Here we report "charge/discharge" properties of the Li–V–Si–O thin film, aiming at utilizing redox reactions of multivalent vanadium ions. Following the results, the feasibility of applying the Li–V–Si–O films as high-voltage negative electrode materials is discussed (Yada et al., 2006).

Characterization of a pristine Li–V–Si–O thin solid electrolyte film.

An XRD pattern of the pristine Li–V–Si–O thin film showed no characteristic peaks other than those originating from the substrate, indicating that no crystalline phase was confirmed in the film. Figure 2 shows a Cole-Cole plot of an ionically blocking cell, Pt/Li–V–Si–O/Pt, measured at 298 K. The spectrum consisted of one semicircle in the higher frequency region followed by a nearly vertical tail, suggesting that the electrical conductivity of the film is fairly dominated by ionic conduction. The semicircle can be assigned to the ionic conduction in the Li–V–Si–O thin solid electrolyte film, whose characteristic frequency was ca. 10 kHz.

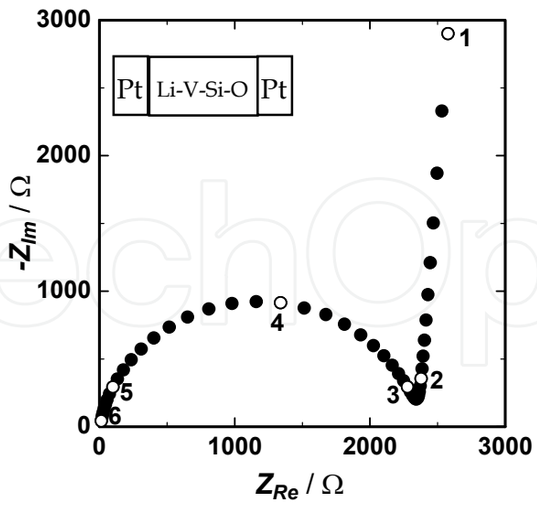

Fig. 2. Cole-Cole plot of Pt/Li-V-Si-O/Pt (750 nm in thickness, 0.25 cm^2 in electrode area) measured at 298 K. Open circles are data points obtained at 10^n Hz, where n is denoted near the open circles.

The ionic conductivity of the film at 298 K was $1.3x10^{-7}$ S cm^{-1}. The electronic contribution to the total electric conductivity was evaluated by two-electrode dc polarization technique, indicating that the transference number of lithium ions in the film was almost unity. The activation energy for ionic conduction in the film was 56.5 kJ mol^{-1}. These results are in good agreement with the previous reports.

Charge/discharge properties of a Li–V–Si–O thin solid electrolyte film.

Although the prepared thin films can work well as solid electrolytes in appropriate potential region, once the potential exceeds over the limitation of potential windows, they are irreversible decomposed. Here, electrochemical properties of the reductively decomposed material as an anode material and its decomposition process will be discussed below.

Figure 3(a) and (b) shows typical charge/discharge profiles of the Li–V–Si–O thin solid electrolyte film obtained at 12.8 μA cm^{-2} in the 1st and 47th cycles and at 2.55 μA cm^{-2} in the 48th and 90th cycles, respectively. The OCV of the film electrolyte before the charge/discharge reaction was 2.8 V. In the first discharge, the electrode potential dropped steeply from the OCV to ca. 1.7 V, followed by an asymptotic potential decrease to 1.0 V with a capacity of 3.8 μAh cm^{-2}. In the first charge, however, the potential rapidly increased and immediately reached 4.0 V, whose capacity was only 0.8 μAh cm^{-2}. The difference between the discharge and charge capacities observed at the first cycle, 3.0 μAh cm^{-2}, would be consumed to decompose the Li–V–Si–O thin solid electrolyte film. In the subsequent charge/discharge cycles, the difference in the discharge and charge capacities, irreversible capacity, gradually decreased with the repetition of the charge/discharge reaction. At the 47th cycle, the irreversible capacity became very small and the reversible charge/discharge capacity increased to 2.6 μAh cm^{-2}. When the current density was decreased to 2.55 μA cm^{-2}, Figure 3(b), the discharge and charge capacities increased to 20 and 13 μAh cm^{-2}, respectively, and the irreversible capacity was observed again. This would be attributed to much more decomposition of the film electrolyte due to the smaller overpotential resulting from the smaller current density. In the prolonged cycles, both the discharge and charge capacities constantly increased and achieved 58 and 52 μAh cm^{-2}, respectively, at the 90th cycle. The increase in the capacities was brought by microstructural reformation of the film, as is discussed later. Figure 4 summarizes the variation in the charge/discharge capacities of the film as a function of the cycle number. Obvious increases in the charge/discharge capacities were observed during the 48th–90th cycles. When the current density was increased to 12.8 μA cm^{-2} again (91st–108th cycles), the charge/discharge capacities maintained almost the same value, 38 μAh cm^{-2}, which was ca. 10 times larger than that obtained at the 1st–47th cycles. When the current density was decreased to 2.6 μA cm^{-2} (109th–119^{th} cycles) again, the charge/discharge capacities did not increase further and showed almost the same value of 60 μAh cm^{-2}.

SEM images revealed that the Li–V–Si–O thin film became rough after the charge/discharge measurement. This micro structural reformation would be due to stress relaxation of the film by the repetition of lithium insertion/extraction reaction. Also, XPS analysis revealed that mean valence of vanadium decrease, indicating that the valence change of vanadium concerns with the redox reaction. In the pristine film, asymmetric peaks of V 2p1/2 at around 523 eV and V 2p3/2 at around 516 eV, which can be deconvoluted to peaks originating from V5+ and V4+ was observed. On the other hand, the film retained at 1.0 V

gave lower binding energies, meaning the presence of lower oxidation number (+2.5) than the pristine film.

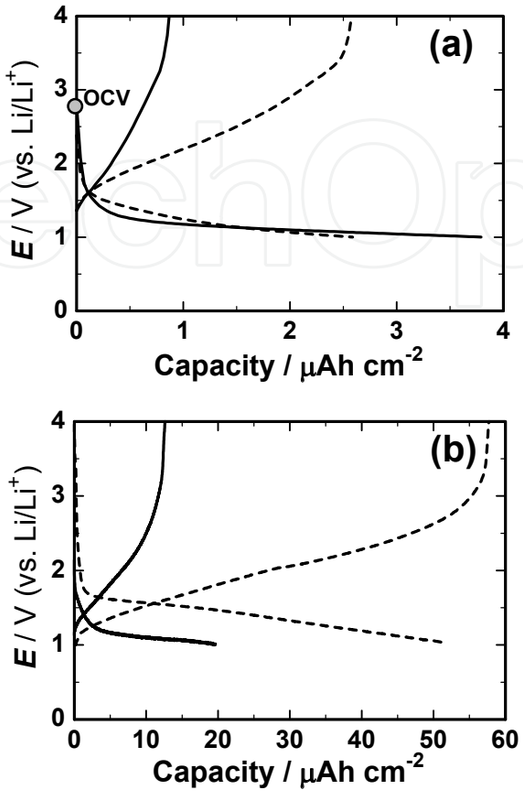

Fig. 3. (a) Charge/discharge profiles of Li-V-Si-O thin film obtained at a current rate of 12.8 μA cm^{-2} in (-)1st cycle and (---)47th cycle. (b) Charge/discharge profiles of Li-V-Si-O thin film obtained at a current rate of 2.55 μA cm^{-2} in (-)48th cycle and (---)90th cycle.

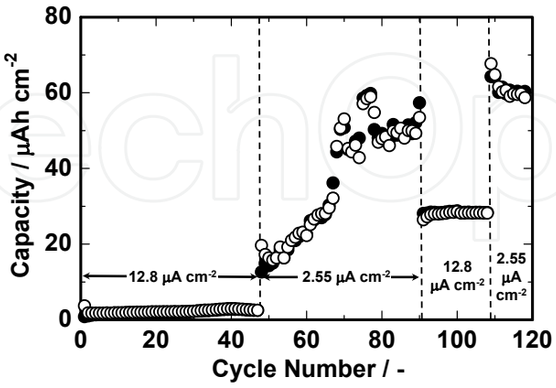

Fig. 4. (●)Charge and (○)discharge capacities as a function of cycle number for Li-V-Si-O thin film obtained at current rates of 12.8 μA cm^{-2} and 2.55 μA cm^{-2}. Cutoff voltages are 1.0 and 4.0 V (vs. Li/Li+).

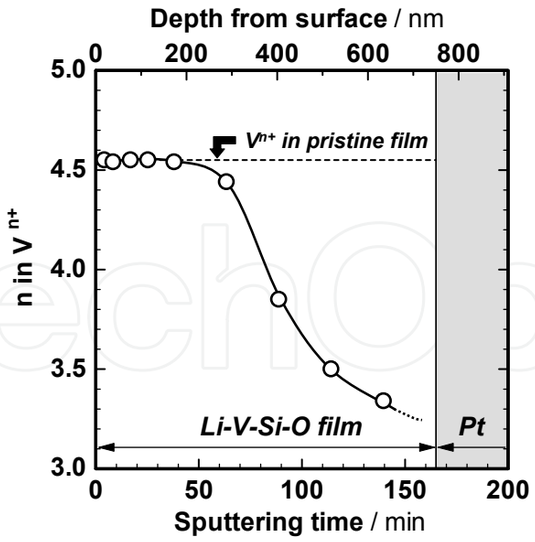

Fig. 5. Depth profile of average oxidation state of vanadium-ions in partially decomposed Li-V-Si-O thin film.

In order to investigate this decomposition process of the Li–V–Si–O thin solid electrolyte film, XPS analysis was conducted to a partially decomposed Li–V–Si–O thin film, which was prepared by applying current of 2.55 μA cm^{-2} reductively until the electrode potential reached 1.0 V. The depth profile of average oxidation numbers of vanadium ions is summarized in Figure 5. The V 2p binding energies maintained their initial state until the middle of the thin film; the average oxidation number of vanadium ions kept the initial state. However, they gradually shifted to the lower energy levels as ion milling time increased, indicating that the average oxidation number of vanadium ions gradually decreased toward the depth direction. These results indicate that the decomposition of the Li–V–Si–O thin solid electrolyte film started from the current collector side. Because charge/discharge reaction was available for the partially decomposed film as well, the part in the vicinity of the current collector performed as an electrode material. This result indicates that both an electrode material and a solid electrolyte coexisted in the partially decomposed Li–V–Si–O thin film.

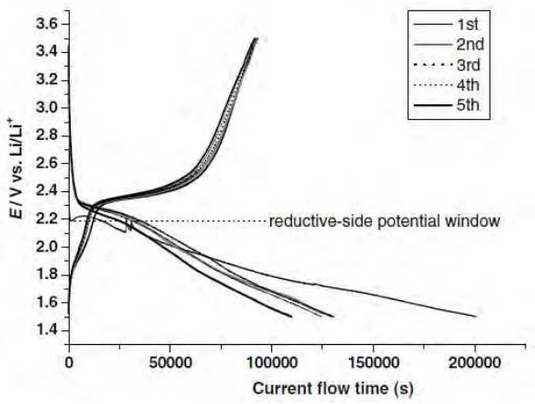

Fig. 6. Charge–discharge curves of Cu/OHARA sheet in 1 mol dm^{-3} $LiClO_4$ dissolved in propylene carbonate between 3.5 and 1.5 V. I = 1.0 μA.

2.2.2 Li-Al-Si-Ti-O system

As with the case of Li-V-Si-O system, crystalline-glass electrolyte (Li-Al-Si-Ti-O system) also shows interesting reductive decomposition reaction. The glass electrolyte sheet with 150 μm in thickness obtains $1x10^{-4}$ S cm^{-1} in its Li^+ conductivity at room temperature, and its activation energy for the Li^+ conduction in the bulk is 30 kJ mol^{-1}, which was manufactured by Ohara Inc. Electrochemical lithium insertion/extraction reaction of the OHARA sheet was investigated using a three-electrode cell. Working electrode was the Cu film deposited on one side of the OHARA sheet. Opposite side of the OHARA sheet was bare. The counter and reference electrodes were lithium metal. The liquid electrolyte, propylene carbonate (PC) containing 1 mol dm^{-3} $LiClO_4$, was filled only into bare side of the OHARA sheet. Electrochemical lithium insertion/extraction reaction of the OHARA sheet was carried out at a constant current of 2.5 μA cm^{-2} in an argon-filled glove box.

Figure 6 shows charge–discharge curve of the "OHARA sheet". The charging process (lithium insertion reaction) at first cycle starts at 2.2 V (vs. Li/Li^+). This potential generally considers as reductive-side potential window of the OHARA sheet. After that, the potential gradually decreased with increasing current flow time from 2.2 to 1.6 V. In the discharge process (lithium extraction reaction) at first cycle, potential plateau was clearly observed at 2.3 V. This discharge capacity was smaller than that of the charging capacity, indicating that the charge–discharge reaction at first cycle is not reversible reaction but includes some irreversible reactions. This irreversible reaction will be responsible for decomposition reaction of the OHARA sheet, and the resultant decomposition material becomes an insertion electrode material operating at 2.3 V vs. Li/Li^+. The charge–discharge capacities were preserved after the second cycles.

The pristine OHARA sheet is white color. The OHARA sheet after the charge–discharge reaction maintained its initial color at the organic electrolyte side while the current collector (Cu) side became dark blue. This dark blue region never returned to its pristine white color even after maintaining its open circuit voltage. This indicates that the dark blue region was irreversibly formed in the OHARA sheet only around Cu current collector. It will be reasonable to expect that this dark blue region is the decomposition material formed at the first charging process and that this region can act as the electrode material. XPS analysis showed that reduced Ti peak was observed at the blue colored region, and this Ti will work as the redox species in the in-situ formed electrode material.

Both Li-V-Si-P-O glass electrolyte and Li-Al-Si-Ti-O crystalline glass sheet start gradual reductive decomposition reaction from current collector side. This decomposition process is not universal phenomena in solid electrolytes and seems to strongly depend on the species of solid electrolytes.

3. Thin-film type batteries with *in-situ* formed materials

As mentioned above, reductively decomposed material of solid electrolyte works as lithium insertion material. Here, manufacturing examples using in-situ formed material in all-solid-state battery system on one side (Iriyama et al., 2006) or both sides (Yada et al., 2009) will be shown below, where OHARA sheet was mainly used as a model solid electrolyte.

3.1 Battery with in-situ formed electrode material on one side

Amorphous lithium manganese oxide thin film was deposited to one side of the sheet by pulsed laser deposition at room temperature. After that, metal film of Pt was deposited on it as a current collector by r.f. magnetron sputtering. Subsequently, metal film of Cu was deposited on the opposite side as a current collector by the sputtering, and a layer of Cu/OHARA sheet/amorphous Li–Mn–O/Pt was fabricated. Voltage of the resultant layer was 0 V. A D.C. 400 V was applied to the resultant layer for a few seconds at room temperature, where Cu side was connected to cathode and Pt side to anode. After the high voltage application, voltage of the layer gradually decreased with time and, finally, it stabilized at 1.7 V. Charge–discharge reaction of the resultant ''all-solid-state thin-film-type lithium-ion battery'' was conducted by 1 μA cm^{-2} between 2.2 and 1.0 V at room temperature. Figure 7(a) shows a plausible fabrication scheme of this battery.

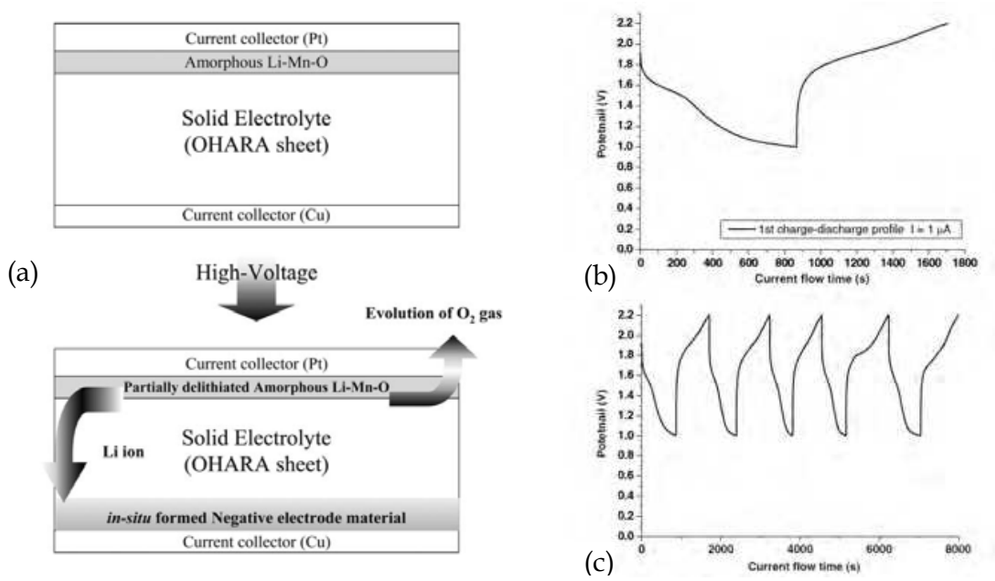

Fig. 7. (a)A plausible fabrication scheme for all-solid-state rechargeable lithium-ion battery (Cu/OHARA sheet/amorphous Li–Mn–O/Pt) developed by applying D.C. high voltage. Charge–discharge curves of the above battery developed by applying D.C. high voltage: (b) charge–discharge curve at first cycle and (b) sequential charge–discharge curves. I = 1.0 μA.

Figures 7(b) and 7(c) show charge–discharge cycles of the resultant all-solid-state thin-film-type lithium-ion battery between 1.0 and 2.2 V. As shown in Fig. 7(b), this battery obtained charge–discharge reaction at around 1.4 V. The irreversible capacity at first cycle was small, and the battery could repeat stable charge–discharge reaction as shown in Fig. 7(c). The charge–discharge reaction of OHARA sheet proceeds at 2.3 V vs. Li/Li^+ as shown in Fig. 6. On the other hand, electrochemical lithium insertion/extraction reaction of amorphous Li–Mn–O occurs at around 3.7 V (Yokoyama et al., 2003). Hence, operating voltage of the resultant battery will be due to the difference of redox potential of these two electrodes.

Cross-sectional SEM image revealed interesting structural change. Figures 8(a) and 8(b) illustrate the cross-sectional SEM images at the amorphous Li–Mn–O/OHARA sheet interface before and after applying the high voltage, respectively. As shown in Fig. 8(a), the as-deposited amorphous Li–Mn–O film electrode was composed of fine particles and these

particles mounted densely on the OHARA sheet. Once the high voltage was applied on the layer, some of cavities were clearly formed at around the amorphous Li–Mn–O/OHARA sheet interface as shown in Fig. 8(b). The cavities seemed to be formed mainly in the amorphous Li–Mn–O film electrode. In addition, the amorphous Li–Mn–O thin film became smooth after applying the high voltage, which may be due to resistive heat generated by applying the high voltage. Figs. 8(c) and 8(d) show the cross-sectional SEM images at the Cu/OHARA sheet interface, respectively. In comparison with the OHARA sheet/amorphous Li–Mn–O interface, the Cu/OHARA sheet interface did not show clear differences before and after applying the high voltage.

As mentioned above, all-solid-state thin-film-type lithiumion battery with in situ formed negative electrode material can be prepared by applying a D.C. high voltage to a Cu/OHARA sheet/amorphous Li–Mn–O/Pt layer. The OHARA sheet around the Cu current collector decomposed irreversibly by application of the high voltage, resulting in negative electrode material in situ formed at Cu/OHARA sheet interface. This negative electrode material obtained reversible charge–discharge capacity in the potential window of the original OHARA sheet. Also, at positive electrode side, oxidation reaction of oxygen ions will occur around the electrode/solid electrolyte interface in addition to the lithium extraction from amorphous Li–Mn–O. It is suggested that oxidation current due to the oxidation reaction of oxygen ions compensated reduction current required to form the negative electrode material. The resultant all-solid state thin-film-type lithium-ion battery operated at 1.4 V, repeated stable charge–discharge reaction, and obtained reversible charge–discharge capacity from the initial charge–discharge cycle.

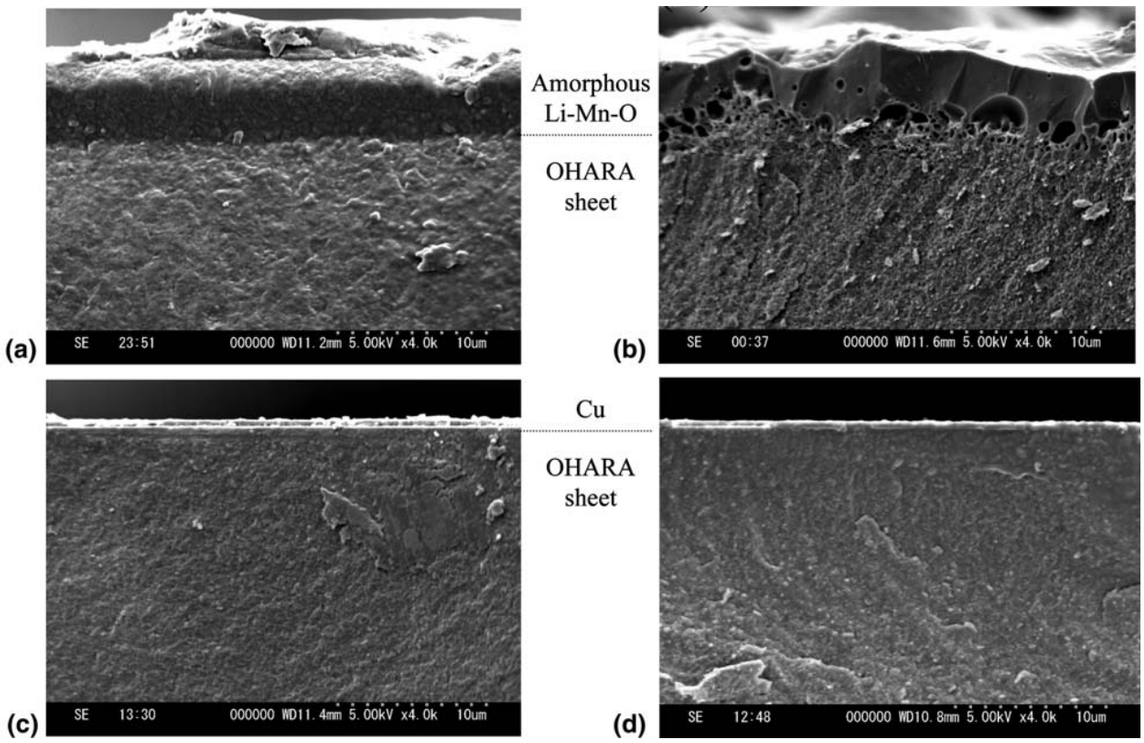

Fig. 8. Cross-sectional SEM images of amorphous Li–Mn–O/OHARA sheet interface: (a) before and (b) after applying D.C. high voltage. Cross-sectional SEM images of OHARA sheet/Cu interface: (c) before and (d) after applying D.C. high voltage.

In-situ preparation of positive electrode material has been investigated using LiPON films (Iriyama et al, 2008). In this case, electrochemical oxidation of iron and the iron ions diffusion into LiPON film was used to fabricate *in-situ* formed iron phosphate amorphous electrode. Although the interfacial resistance at the resultant *in-situ* formed electrode/LiPON interface became smaller than that at the amorphous lithium iron-phosphate/LiPON interface where the film electrode was deposited on LiPON film by PLD, the resultant batter obtained quite small capacity. This is probably because of the difficulty of iron ions diffusion into internal region of LiPON film.

3.2 Battery with *in-situ* formed electrode materials on both sides

In the previous system, electrode material on one side was prepared by in-situ process. In case of negative electrode side, the electrode active material was reductively decomposed material from the solid electrolyte (OHARA sheet) and formed only around the Cu current collector. However, only one electrode active material was prepared. Preparation of both electrodes by in-situ process would simplify the fabrication process markedly. In this paper, a novel all-solid-state battery with in-situ formed electrodes on both sides.

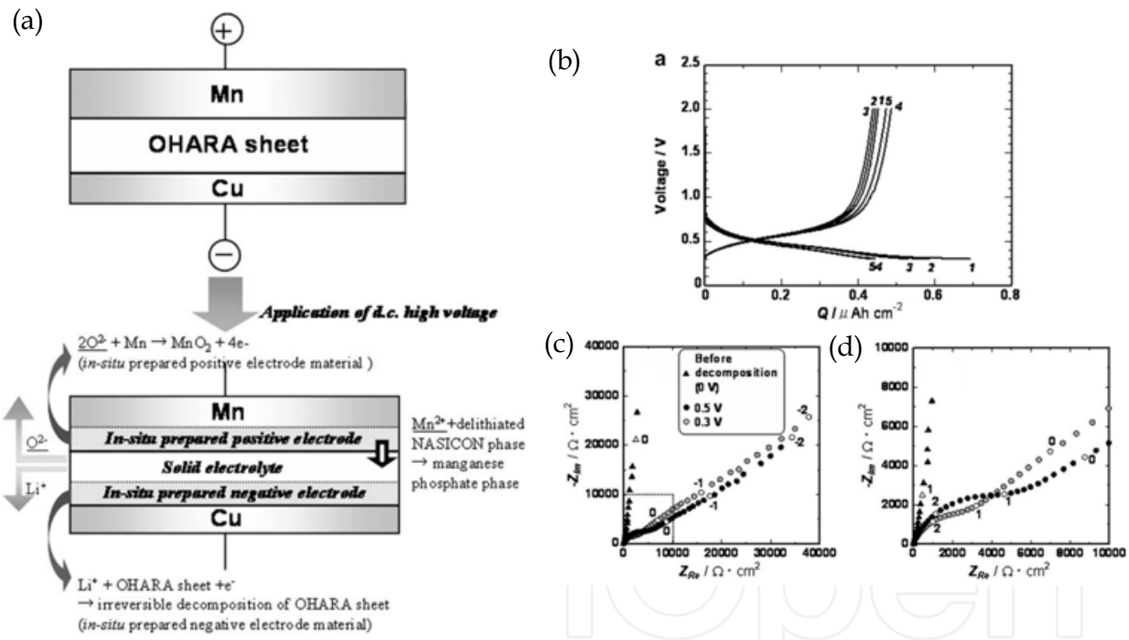

Fig. 9. (a) Charge–discharge profiles of an all-solid-state Cu/OHARA sheet/Mn battery (electrode area: 0.15 cm^2, thickness: 0.03 cm). I = 0.33 μA cm^{-2}. Cycle numbers are denoted at the end of the charge–discharge curves. (b) Cole-Cole plots of the Cu/OHARA sheet/Mn battery. Magnified image of high frequency region in (b) (surrounded by dotted square) is shown in (c). Open symbols are data points obtained at 10^n Hz, where n is denoted near the open symbols.

A layer of Cu metal film/OHARA sheet/Mn metal film shown in Fig. 9 was fabricated in the following manner. Thin-film of Cu (thickness: 0.5 μm, area: 0.15 cm^2) was deposited on one side of the OHARA sheet by r.f. magnetron sputtering method with r.f. power of 40W

under argon atmosphere (1.5 Pa). After that, Mn thin-film (thickness: 1.5 μm, area: 0.15 cm^2) was deposited on the other side of the OHARA sheet by vacuum evaporation. D.c. 16 V was applied to the resultant Cu/OHARA sheet/Mn layer for 10 h at 353 K in air, where the Cu side was connected to cathode and the Mn side to anode. This high voltage application made the layer to a Cu/OHARA sheet/Mn battery. A plausible battery preparation scheme is shown in Fig. 9(a). Hereafter, as-prepared Cu/OHARA sheet/Mn layer and the resultant Cu/OHARA sheet/Mn battery are referred to as COM layer and COM battery, respectively. Figure 9(b) shows the charge–discharge profiles of the COM battery between 0.3 V and 2.0 V. A clear charge–discharge capacity was observed at 0.3–0.8 V, while the COM layer did not have any capacity in this voltage range. The irreversible capacity was ca. 0.25 μAh cm^{-2} at the initial cycle and decreased with repetition of the charge–discharge reactions. A stable, reversible capacity of 0.45 μAh cm^{-2} was observed at the fifth cycles. Figs. 9(c) and 9(d) show Cole-Cole plots of the COM battery measured at 0.3 and 0.5 V. Cole-Cole plot of the COM layer is also displayed in these figures for comparison. The Cole-Cole plot of the COM layer consisted of a nearly vertical line to the real axis with a resistive component (20 Ω cm^2) in the high frequency region. The resistive component was assigned to the resistance of the OHARA sheet. This result indicates that both the Cu and Mn metal films performed as ionically blocking electrodes. On the other hand, Cole-Cole plots of the COM battery showed a depressed semicircular arc in the middle frequency region (10 Hz < f < 100 kHz) together with a slope of nearly 45° to the real axis in the low frequency region (f < 10 Hz).
The diameter of this semicircular arc depended on the cell voltage, suggesting that this semicircular arc contains charge transfer resistances at the in situ prepared electrodes/solid electrolyte interface. The slope of nearly 45° observed at lower frequency region would correspond to Warburg impedance in the in situ prepared electrode materials. This result supports that the electrode active materials are prepared at both sides just by applying d.c. high voltage to COM layer. As shown in Fig. 9(a), the in-situ prepared negative electrode material will be a partially decomposed OHARA sheet around the Cu current corrector as discussed in previous section. In this preparation process, excess Li^+ is required to decompose the OHARA sheet irreversibly for the fabrication of the negative electrode material. The Li^+ source for the reductive decomposition is restricted to the OHARA sheet itself. Therefore, to promote Li^+ migration in the OHARA sheet to the Cu side so that Li^+ is consumed in the irreversible preparation of the negative electrode material, charge compensation is necessary at the positive electrode side in the OHARA sheet. One of the most significant reactions would be the release of oxygen ions from the OHARA sheet at the positive electrode side. If the released oxygen ions react with the Mn film at the OHARA sheet/Mn interface, formation of a manganese oxide will be expected. Once the dense MnO_2 phase is formed at the interface, it is speculated that counter diffusion of both manganese ions and oxide ions in the MnO_2 will grow the phase. Such diffusion will not proceed so fast, which will be one of the reasons for the small quantity of the resultant MnO_2 phase. The lithium insertion/extraction reaction to the MnO_2 occurs at ca. 3 V (Thackeray, 1997) and the half cell test also revealed that lithium insertion/extraction reaction at OHARA sheet/Mn film of the COM battery operated at ca. 3.0 V. On the other hand, lithium insertion/extraction reaction to the decomposed OHARA sheet occurs at ca. 2.3 V. Difference of this lithium insertion/extraction potential in these two electrodes will be reasonably agreement with the cell voltage shown in Fig. 9(b). Although oxygen ions in the OHARA sheet will interact strongly with phosphorus to form PO_4, free energy change for

the oxidation reaction of Mn has a relatively large negative value (Kubaschewski, 1978), which can promote the release of oxygen ions. XRD showed that Mn layer in the COM battery was mainly Mn metal and could not detect such manganese oxide phase, but this will be probably because of its small quantity. Another possibility that should be considered will be an oxidation of Mn and formation of a manganese phosphate phase due to the migration of Mn^{2+} into the OHARA sheet. The crystalline part of the OHARA sheet is mainly the composition of $LiTi_2(PO_4)_3$, where lithium locate at M1 site in the structure. Aatiq et al. have pointed out that Mn^{2+} can occupy the M1 site, resulting in the formation of $(Mn_{0.5})M_1Ti_2(PO_4)_3$ phase (Artiq et al., 2001, 2002). They have reported that lithium insertion into the M1 site of $Li_xMn_{0.5}Ti_2(PO_4)_3$ phase leads to a potential plateau in the vicinity of 2.9 V (Li/Li^+) at $0 < x < 0.5$, following to the insertion into the M2 site around 2.2–2.5 V (Li/Li^+). When the lithium content of M1 sites around Mn film decrease due to the migration of Li^+ into Cu film side, a part of Mn^{2+} migration into the M1 sites for the charge compensation may be considerable. However, the lithium insertion process at 2.9 V region was not observed in half cell test. Hence, we consider that this charge–discharge capacity will not contribute so much to the capacity observed in Fig. 9(b).

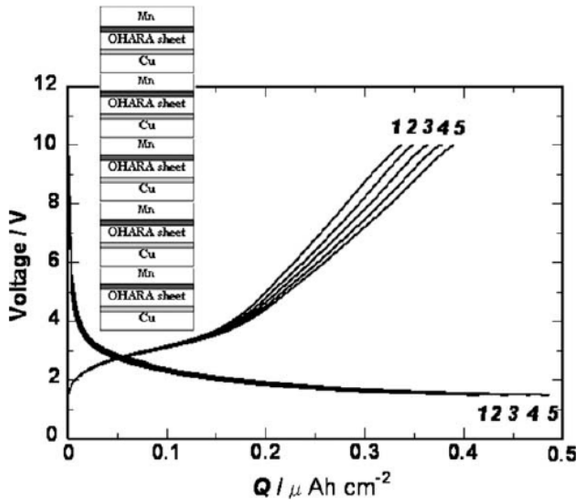

Fig. 10. Charge–discharge profiles of a five-series of all-solid-state Cu/OHARA sheet/Mn battery (electrode area: 0.15 cm^2, thickness: 0.15 cm) measured at 353 K. I = 0.33 μA cm^{-2}. Cycle numbers are denoted at the end of the charge–discharge curves.

One of the problems of the proposed COM battery is its low usable voltage (0.3–0.8 V), which is too small for practical applications. To overcome this problem, a d.c. 16 V was applied to a series of five COM layers. Charge–discharge profiles of the resultant fiveseries COM batteries are shown in Fig. 10. The battery had charge–discharge reactions of 1.5–4.0 V, which was five times larger voltage than that of the single battery. This result indicate that COM batteries with high voltages can be easily fabricated by stacking many layers serially and applying appropriate d.c. high voltage to promote the in situ fabrication of electrode active materials at the positive and negative sides. The energy density per unit cell can be simply increased by reducing the thickness of solid electrolyte. Our calculation indicates that a cell made with an OHARA sheet (5.0 μm in thickness) has an energy density of ca. 0.1 Wh kg^{-1}, which is nearly equivalent to that of the popular electrolytic capacitor. It is true that

the capacity of the COM battery is also small, but this will be improved by increasing the interface region, for example using three-dimensional porous solid electrolyte with high surface area (Kanamura et al., 2005).

4. Conclusion

In this chapter, new kinds of all-solid-state Li-ion battery with in-situ formed electrode material were introduced. Generally, decomposition reaction of solid electrolytes has considered as a limitation of voltage, the resultant decomposed material sometimes work as in-situ formed electrode materials. In addition, when the decomposed materials grow uniformly from the current collector, solid electrolyte/electrode interface can be formed by in-situ process that can be used in all-solid-state batteries. Because the large resistance at the electrode/solid electrolyte interface is a crucial problem to develop high power all-solid-state lithium-ion batteries, this novel fabrication process may become an effective method to reduce the interfacial resistance. However, in the current stage, this proposed battery does not obtain sufficient electrochemical properties, typically, on capacity, reaction rate, and voltage. To overcome these problems, mechanism of decomposition reaction of solid electrolytes and their characterization should be fundamentally clarified, which are currently investigated.

5. References

Aatiq, A.; Delmas, C.; El Jazouli, A. (2001). Structural and electrochemical study of $Li_{0.5}Mn_{0.5}Ti_{1.5}Cr_{0.5}(PO_4)_3$. *Journal of Solid State Chemistry*, Vol. 158, No. 2, p169-174, 0022-4596.

Aatiq, A.; Menetrier, M.; El Jazouli, A. & Delmas, C. (2002). Structural and lithium intercalation studies of $Mn_{(0.5-x)}Ca_xTi_2(PO_4)_3$ phases ($0<x<0.50$). *Solid State Ionics, Diffusion & Reactions*, Vol. 150, No. 3-4, p. 391-405, 0167-2738.

Aono, H.; Sugimoto, E.; Sadaoka, Y.; Imanaka, N. & Adachi, G. (1989). Ionic conductivity of the lithium titanium phosphate ($Li_{1+x}MxTi_{2-x}(PO_4)_3$, M=Al, Sc, Y, and La) systems. *Journal of the Electrochemical Society*, Vol. 136, No. 2, p590-591, 0013-4651.

Aono, H.; Sugimoto, E.; Sadaoka, Y.; Imanaka, N. & Adachi, G. (1990). Ionic conductivity of solid electrolytes based on lithium titanium phosphate. *Journal of the Electrochemical Society*, Vol. 137, No. 4, p1023-1027, 0013-4651.

Bates, J. B.; Dudney, N. J.; Gruzalski, G. R.; Zuhr, R. A.; Choudhury, A.; Luck, C. F. & Robertson, J. D. (1993). FABRICATION AND CHARACTERIZATION OF AMORPHOUS LITHIUM ELECTROLYTE THIN-FILMS AND RECHARGEABLE THIN-FILM BATTERIES. *Journal of Power Sources*, Vol. 43, No.1-3, p. 103-110, 0378-7753.

Birke, P.; Scharner, S.; Huggins, R. A. & Weppner, W. (1997), Electrolytic stability limit and rapid lithium insertion in the fast-ion-conducting $Li_{0.29}La_{0.57}TiO_3$ perovskite-type compound, *Journal of the Electrochemical Society*, Vol. 144, No. 6, pL167-L169, 0013-4651.

Fu, J. (1997). Fast Li^+ ion conduction in Li_2O-Al_2O_3-TiO_2-SiO_2-P_2O_5 glass-ceramics. *Journal of the American Ceramic Society,* Vol. 80, No. 7, p1901-1903, 0002-7820.

Glass, A.M.; Nassau, K. & Negran, T. J. (1978). Ionic conductivity of quenched alkali niobate and tantalate glasses. *Journal of Applied Physics*, Vol. 49, No. 9, p4808-4811, 0021-8979.

Greatbatch, W.; Lee, J. H.; Mathias, W.; Eldridge, M.; Moser, J. R. & Schneider, A. A.(1971) *IEEE Transactions on Biomedical Engineering*, Vol. BME-18, No. 5, p317-324, 0018-9294.

Hong, H. Y. P. (1978). Crystal structure and ionic conductivity of $Li_{14}Zn(GeO_4)_4$ and other new Li^+ superionic conductors. *Materials Research Bulletin,* Vol. 13, No. 2, p117-124, 0025-5408.

Inaguma, Y.; Liquan, C.; Itoh, M.; Nakamura, T.; Uchida, T.; Ikuta, H. & Wakihara, M. (1993). High ionic conductivity in lithium lanthanum titanate. *Solid State Communications*, Vol. 86, No. 10, p689-693, 0038-1098.

Iriyama, Y.; Yada, C.; Abe, T.; Ogumi, Z. & Kikuchi, K. (2006). A new kind of all-solid-state thin-film-type lithium-ion battery developed by applying a DC high voltage. *Electrochemistry Communications*, Vol. 8, No. 8, p1287-1291, 1388-2481.

Iriyama, Y.; Shimidu, D.; Abe, T.; Sudoh, M.; & Ogumi, Z. (2008). Fast and Stable Charge Transfer Reaction at the $Li_{4/3}Ti_{5/3}O_4$/Lithium Phosphorus Oxynitride (LIPON) Interface and its Application to All-Solid-State Thin Film Batteries, ECS Transactions of 214th ECS Joint Meeting "PRiME 2008", p45-52, Vol. 16, No. 26, Honolulu, Oct. 12-17, 2008, ECS.

Kanamura, K.; Akutagawa, N. & Dokko, K. (2005). Three dimensionally ordered composite solid materials for all solid-state rechargeable lithium batteries. *Journal of Power Sources*, Vol. 146, No. 1-2, p86-89, 0378-7753.

Kawamura, J.; Kuwata, N.; Toribami, K.; Sata, N.; Kamishima, O. & Hattori, T. (2004). Preparation of amorphous lithium ion conductor thin films by pulsed laser deposition. *Solid State Ionics, Diffusion & Reactions*, Vol. 175, No. 1-4, p273-276, 0167-2738.

Kubaschewski, O. & Alcock C. B. (1979). *Metallurgical Thermochemistry, fifth ed.,* Pergamon Press, 0080208975, New York.

Kuwano, J. & West, A.R. (1980). New Li^+ ion conductors in the system, Li_4GeO_4-Li_3VO_4. *Materials Research Bulletin*, Vol. 15, No. 11, p1661-1667, 0025-5408.

Malugani, J.P. & Robert, G. (1979). Ionic conductivity of the glasses $LiPO_3$-LiX(X=I, Br, Cl). *Materials Research Bulletin*, Vol. 14, No. 8, p.1075-1081, 0025-5408 .

Neudecker, B. J.; Dudney, N. J. & Bates, J. B. (2000). "Lithium-free" thin-film battery with in situ plated Li anode. *Journal of the Electrochemical Society*, Vol. 147, No. 2, p517-523, 0013-4651.

Ohtsuka, H. & Yamaki, J. (1989). Electrical characteristics of Li_2O-V_2O_5-SiO_2 thin films. *Solid State Ionics, Diffusion & Reactions*, Vol. 35, No. 3-4, p201-206, 0167-2738.

Rabenau, A. (1982). Lithium nitride and related materials case study of the use of modern solid state research techniques. *Solid State Ionics*, Vol. 6, No. 4, p277-293, 0167-2738.

Radzilowski, R. H.; Yao, Y. F. & Kummer, J. T. (1969). Dielectric loss of beta alumina and of ion-exchanged beta alumina. *Journal of Applied Physics,* Vol. 40, No. 12, p4716-4725, 0021-8979.

Sigaryov, S.E. & V.G. Terziev. (1993). Thermally induced lithium disorder in $Li_3Fe_2(PO_4)_3$. *Physical Review B (Condensed Matter)*, Vol. 48, No. 22, p16252-16255, 0163-1829.

Subramanian, M.A.; Subramanian, R. & Clearfield, A. (1986). Lithium ion conductors in the system AB(IV) $_2(PO_4)_3$ (B=Ti, Zr and Hf). *Solid State Ionics, Diffusion & Reactions,* Vol. 18-19, p562-569, 0167-2738 .

Thackeray, M.M. (1997). Manganese oxides for lithium batteries. *Progress in Solid State Chemistry*, Vol. 25, No. 1-2, p1-71, 0079-6786.

Wang, B.; Bates, J. B.; Hart, F. X.; Sales, B. C.; Zuhr, R. A. & Robertson, J. D. (1996) Characterization of thin-film rechargeable lithium batteries with lithium cobalt oxide cathodes, *Journal of the Electrochemical Society*, Vol. 143, No.10, p3203-3213, 0013-4651.

Yada, C.; Iriyama, Y.; Abe, T.; Kikuchi, K. & Ogumi, Z. (2006). Amorphous Li-V-Si-O thin films as high-voltage negative electrode materials for thin-film rechargeable lithium-ion batteries. *Journal of the Electrochemical Society*, Vol. 153, No. 6, pA1148-A1153, 0013-4651.

Yada, C.; Iriyama, Y.; Abe, T.; Kikuchi, K. & Ogumi, Z. (2009). A novel all-solid-state thin-film-type lithium-ion battery with in situ prepared positive and negative electrode materials. *Electrochemistry Communications*, Vol. 11, No. 2, p413-416, 1388-2481.

Yokoyama, M.; Iriyama, Y.; Abe, T. & Ogumi, Z. (2003). Dependency on the electrode species of Li ion transfer at the electrode/glass electrolyte (LiPON) interface, *Proceedings of the 44th Battery Symposium*, p290-291, Osaka, November, Seiei, Ohsaka.

IntechOpen

Lithium-ion Batteries

Edited by Chong Rae Park

ISBN 978-953-307-058-2
Hard cover, 132 pages
Publisher InTech
Published online 01, April, 2010
Published in print edition April, 2010

There have been numerous excellent books on LIBs based on various different viewpoints. But, there is little book available on the state of the art and future of next generation LIBs, particularly eventually for EVs and HEVs. This book is therefore planned to show the readers where we are standing on and where our R&Ds are directing at as much as possible. This does not mean that this book is only for the experts in this field. On the contrary this book is expected to be a good textbook for undergraduates and postgraduates who get interested in this field and hence need general overviews on the LIBs, especially for heavy duty applications including EVs or HEVs.

InTech Europe
University Campus STeP Ri
Slavka Krautzeka 83/A
51000 Rijeka, Croatia
Phone: +385 (51) 770 447
Fax: +385 (51) 686 166
www.intechopen.com

InTech China
Unit 405, Office Block, Hotel Equatorial Shanghai
No.65, Yan An Road (West), Shanghai, 200040, China
中国上海市延安西路65号上海国际贵都大饭店办公楼405单元
Phone: +86-21-62489820
Fax: +86-21-62489821

IntechOpen